The Immunological Synapse: A Molecular Machine Controlling T Cell Activation

Arash Grakoui; Shannon K. Bromley; Cenk Sumen; Mark M. Davis; Andrey S. Shaw; Paul M. Allen; Michael L. Dustin

Science, New Series, Vol. 285, No. 5425. (Jul. 9, 1999), pp. 221-227.

Stable URL:
http://links.jstor.org/sici?sici=0036-8075%2819990709%293%3A285%3A5425%3C221%3ATISAMM%3E2.0.CO%3B2-K

Science is currently published by American Association for the Advancement of Science.

The Immunological Synapse: A Molecular Machine Controlling T Cell Activation

Arash Grakoui,[1] Shannon K. Bromley,[1] Cenk Sumen,[2] Mark M. Davis,[2] Andrey S. Shaw,[1] Paul M. Allen,[1] Michael L. Dustin[1]*

The specialized junction between a T lymphocyte and an antigen-presenting cell, the immunological synapse, consists of a central cluster of T cell receptors surrounded by a ring of adhesion molecules. Immunological synapse formation is now shown to be an active and dynamic mechanism that allows T cells to distinguish potential antigenic ligands. Initially, T cell receptor ligands were engaged in an outermost ring of the nascent synapse. Transport of these complexes into the central cluster was dependent on T cell receptor–ligand interaction kinetics. Finally, formation of a stable central cluster at the heart of the synapse was a determinative event for T cell proliferation.

A critical event in the initiation of the adaptive immune response is the activation of T lymphocytes. This is mediated by the interaction of T cell antigen receptors (TCRs) with their ligands, major histocompatibility molecule–peptide complexes (MHC-peptide) (*1*). Within seconds of MHC-peptide engagement, the TCR initiates a tyrosine phosphorylation cascade that triggers multiple branching signaling pathways (*2*). These early signals may be sufficient to trigger some effector functions, such as killer T cell execution of target cells. In contrast, more complex functions, such as T cell proliferation, require TCR engagement and signaling for many minutes or hours. The mechanisms of sustained TCR engagement are, however, not well understood.

Sustained TCR engagement, although essential for T cell activation, faces many barriers. First, TCR engagement is impeded by the small size of the TCR and MHC molecules. Large, abundant glycoproteins like CD43 and CD45 impose a steric barrier to the interaction of TCR and MHC (*3*). Second, the TCR has a low affinity for antigenic MHC-peptide (*4*, *5*). Third, the number of antigenic complexes on the antigen-presenting cell (APC) can be very low (*6*). Lastly, the movement of T cells works against sustained recognition of antigen (*7*). These barriers are active throughout the time the T cell interacts with the APC.

MHC-peptide strength plays an important role in sustained signaling and T cell commitment. T lymphocytes display a remarkable ability to evaluate differences in MHC-peptide complexes. Alteration of a single amino acid in an antigenic peptide can have significant and distinct biological effects on the T cell (*8*). Such altered peptide ligands can be classified as strongly activating (agonist), weakly activating (weak agonist), inhibitory (antagonist), or inactive (null) (*4*, *5*). The wide range of biological activities displayed by altered peptide ligands has been correlated with the half-life ($t_{1/2}$) of the TCR–MHC-peptide interaction (*4*, *5*). This discrimination process is evident in early signaling events such as the phosphorylation of the TCR ζ chain and recruitment of the kinase ZAP-70 to the TCR (*9*). It is not known how these early events are related to the sustained signals that determine T cell commitment.

Initial views of antigen-specific T cell junctions have revealed the formation of a specialized contact, termed the immunological synapse (*10*, *11*). The mature immunological synapse is defined by a specific pattern of receptor segregation with a central cluster of TCRs surrounded by a ring of integrin family adhesion molecules (*11*). We hypothesize that the formation of the immunological synapse provides a mechanism for sustained TCR engagement and signaling.

We now report real-time imaging and quantitative analysis of the formation of a functional immunological synapse. We show that T cell activation is reconstituted by MHC-peptide and an adhesion ligand, ICAM-1, in a glass-supported planar bilayer. Dynamic interactions were further probed by fluorescence photobleaching recovery to assess the stability of complexes formed within the synapse. This quantitative analysis has revealed that immunological synapse formation is a multistage process and provides new insights into how MHC-peptide number and TCR-ligand interaction kinetics are translated into T cell activation decisions.

[1]Center for Immunology and the Department of Pathology, Washington University School of Medicine, 660 South Euclid Avenue, St. Louis, MO 63110, USA. [2]Howard Hughes Medical Institute, Stanford University School of Medicine, Palo Alto, CA 94305, USA.

*To whom correspondence should be addressed at the Department of Pathology, Washington University School of Medicine, 660 South Euclid Avenue, Campus Box 8118, St. Louis, MO 63110, USA. E-mail: dustin@immunology.wustl.edu

MHC-Peptide Capture and Clustering in the Immunological Synapse

We first examined the kinetics and pattern of MHC-peptide accumulation in T cell junctions to determine whether specific stages in the formation of immunological synapse could be discerned. We used two different E^k-restricted model antigen systems, moth cytochrome c (MCC) and hemoglobin (Hb). Using two independent TCR systems permitted us to compare, contrast, and confirm key observations.

To provide a T cell activating system for optimal imaging of molecular interactions in the T cell junction, we replaced the APC with planar bilayers containing fluorescently labeled MHC-peptide and ICAM-1 (*12*). The purified MHC-peptide and ICAM-1 were anchored to the bilayer in a manner that allows their free diffusion in the supported bilayer [Web movies 1 and 2 (*13*)] and thus their free rearrangement upon interactions with cellular receptors (*14*, *15*). T cells were prepared from 2B4 or 3.L2 TCR transgenic mice (*16*), and the time course of contact development between a 2B4 T cell and the planar bilayer was observed (Fig. 1, A and B) [Web movies 3 to 6 (*13*)]. The contact area was defined by interference-reflection microscopy (IRM), which allows visualization of close membrane apposition as dark areas. Patterns of receptor interactions were defined by fluorescence images of MHC-peptide (E^k-MCC88-103) (green) and ICAM-1 (red) rearrangement. In the first 0.5 min, T cells stopped migrating and a broad central zone of ICAM-1 accumulation was established. This central zone was bordered by a ring of close apposition of the T cell membrane and planar bilayer (darkest area of IRM image) that was free of accumulated ICAM-1. MHC-peptide engagement by the TCR was detected at the same time only in the outer, closely apposed ring of the junction. This orientation of accumulated MHC-peptide and ICAM-1 was inside-out compared with that defined for the mature immunological synapse. This peripheral TCR engagement was clearly functional based on the concurrent increase in cytoplasmic Ca^{2+} [Web movie 7 (*13*)]. Over the next 5 min, the engaged MHC-peptides moved to the center of the junction to form a central cluster. This mature immunological synapse was then maintained for over an hour (Fig. 1). Although the density of accumulated MHC-peptide and ICAM-1 reached maximal levels in 10 to 20 min (Fig. 1, C and E), the largest number of MHC-peptide complexes were engaged within 5 min and many were lost during formation of the central cluster (Fig. 1, C and D). The pattern of ICAM-1 and MHC-peptide complex accumulation was not al-

tered by inclusion of CD80 or CD48 in the planar bilayers at physiological densities [Web Fig. 1 (*13*)]. MHC-peptide movement was inhibited by cytochalasin D, an inhibitor of actin-based transport. These images and quantitative data illustrated two stages in the formation of an immunological synapse. Stage 1 is junction formation with engagement of MHC-peptide complexes in an outer ring, and stage 2 is the transport of the accumulated MHC-peptide complexes into the central cluster.

Sensitivity of Central Cluster Formation

To determine the relation between initial MHC-peptide density in the bilayer and the final density of MHC-peptide in clusters, we prepared bilayers with constant ICAM-1 density and varied agonist MHC-peptide density (*14*). Immunological synapse formation was compared at high (Fig. 2, A to E) and low density (Fig. 2F) of MHC-peptide and with a null MHC-peptide (Fig. 2G). Low and high densities of agonist MHC-peptide triggered formation of well-organized immunological synapses whereas, as expected, null MHC-peptide did not. Comparison of T cell proliferation and the density of agonist MHC-peptide complexes in the central cluster reveals that optimal proliferation was obtained over a wide range of initial MHC-peptide complex densities (Fig. 2, H and I). Thus, full T cell activation correlated with formation of an immunological synapse with a threshold density of ≥60 molecules per square micrometer of accumulated MHC-peptide complexes. Importantly, 0.2 molecules per square micrometer, the lowest density of agonist MHC-peptide complex that triggers proliferation and synapse formation, was the equivalent of 100 to 200 MHC-peptide complexes per APC, the minimum number of complexes needed to stimulate T cell interleukin-2 (IL-2) production (*17*). Thus, stages 1 and 2 of immunological synapse formation did not require a high MHC-peptide dose and were observed over the same range of MHC-peptide densities required for T cell activation.

MHC-Peptide Strength and Central Cluster Formation

To determine whether MHC-peptide clustering was related to the strength of the MHC-peptide complex, we loaded E^k with well-characterized altered peptides of MCC and Hb (Table 1) and tested for proliferation and immunological synapse formation (*18*). The pattern and density of MHC-peptide and ICAM-1 accumulation were analyzed (Fig. 3, A and B). Null MHC-peptide complexes (N72E) did not accumulate in the junctions, nor did they stop T cell migration [Web movies 8 to 12 (*13*)]. In contrast, all other antigen types (agonist, weak agonist, and antagonist) stimulated MHC-peptide accumulation (Table 1 and Fig. 3, A and B) [Web movies 8 to 12 (*13*)]. Like strong agonists, the weak agonists in both systems formed immunological synapses as defined by the ICAM-1 accumulation pattern, cessation of migration, and central clusters of accumulated MHC-peptide complexes (Table 1 and Fig. 3, A and B, N72T) [Web movies 8 to 12 (*13*)]. However, the density of MHC-peptide complexes accumulated in the central cluster was lower than with the strong agonist ligands (Table 1). Antagonist peptides slowed T cell migration and stimulated accumulation of MHC-peptide complexes at the junctions (Table 1). However, antagonist peptides (N72I and N72A) did not stop T cell migration and also did not form bona fide immunological synapses, which would require a ring of ICAM-1 accumulation around a central cluster of engaged MHC (Fig. 3, A and B) [Web movies 8 to 12 (*13*)]. The density of clustered MHC-peptide complexes and the proportion of cells forming immunological synapses correlated with proliferation in the 3.L2 (Fig. 3C) and 2B4 [Web Fig. 2 (*13*)] systems.

To determine whether the amount of MHC-peptide accumulated in the contacts was related to TCR affinity, we plotted the density of accumulated MHC-peptide complexes against each of the three intrinsic interaction parameters determined by surface plasmon resonance: the association constant (K_a), the on-rate (k_{on}), and the $t_{1/2}$ ($\ln 2/k_{off}$). This was done for each of six ligands for which all data were available. The use of both the 2B4 and 3.L2 systems revealed that the correlation of K_a or k_{on} with accumulated MHC-peptide density was significant within each system, but poor between the two systems (Fig. 3, D and E). In contrast, the correlation of $t_{1/2}$ and accumulated MHC-peptide density was strong both within and across the two distinct TCR systems (Fig. 3F). Thus, stage 2, MHC-peptide transport, is dependent on the $t_{1/2}$ of the TCR interaction with the MHC-peptide complex.

Role of CD4 in Immunological Synapse Formation

CD4 plays an important role in TCR signaling, but the nature of its contribution is not clear (*19*). To address the role of CD4, we capitalized on the fact that 3.L2 transgenic T cells can develop in the absence of CD4. CD4-deficient 3.L2 T cells were prepared from 3.L2 TCR transgenic mice. Unlike their CD4-positive

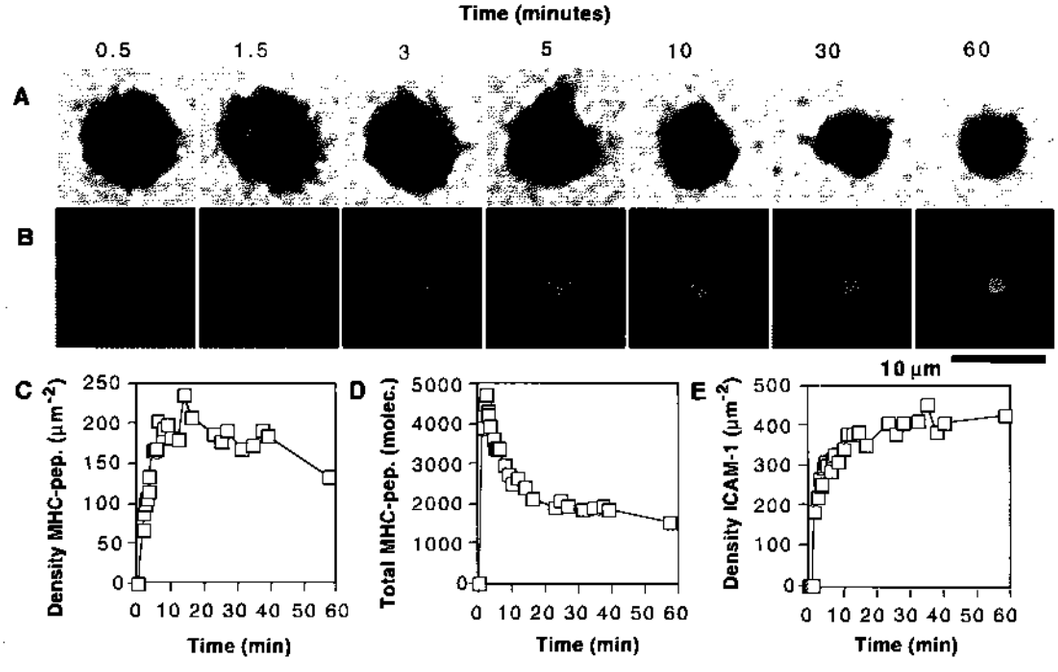

Fig. 1. Formation of the immunological synapse. 2B4 T cells in contact with a supported planar bilayer containing Oregon green E^k(MCC88-103)-GPI at 80 molecules per square micrometer and Cy5 ICAM-1–GPI at 200 molecules per square micrometer. (**A**) Images of contact formation (IRM) at five time points. IRM shows contacts as dark gray on a light background. (**B**) Images of MHC-peptide (green) and ICAM-1 (red) accumulation. (**C**) Density of accumulated E^k(MCC88-103). (**D**) Total accumulated E^k(MCC88-103). (**E**) Density of accumulated ICAM-1. The accumulated ligand measurements were on the entire area where the accumulated ligands exceeded the density in the bilayer (*40*). Original image elements = 0.44 μm². Representative of four experiments with 2B4 and 3.L2.

counterparts, the CD4-negative 3.L2 T cells displayed weak proliferation in response to planar bilayers containing ICAM-1 and the agonist MHC-peptide complex as compared with normal 3.L2 T cells (*20*). They were also much less efficient at stopping and forming immunological synapses (Fig. 4, B compared with A) [Web movies 13 to 15 (*13*)]. CD4-negative 3.L2 T cells interacting with an agonist MHC-peptide complex appeared most similar to CD4-positive 3.L2 T cells on antagonist MHC-peptide complexes in the failure to stop migration and the concomitant lack of mature immunological synapses. Similar results were obtained by treating the CD4-positive 3.L2 cells with a function blocking antibody to CD4 before plating on a bilayer with ICAM-1 and agonist MHC-peptide complexes (Fig. 4C) [Web movies 13 to 15 (*13*)]. Thus, CD4 increases the efficiency of stage 1 of immunological synapse formation, particularly the process of stopping migration.

Dynamics of MHC-Peptide Clusters

To examine the dynamics of interaction between TCR and MHC-peptide complexes in the immunological synapse, we performed fluorescence photobleaching recovery (FPR) experiments (*21*, *22*). We first established the intrinsic dynamics of the TCR–MHC-peptide interaction using Chinese hamster ovary (CHO) cells expressing glycosyl-phosphatidylinositol (GPI)–anchored 2B4 TCRs with bilayers containing fluorescently labeled MHC-peptide complexes. The CHO cells formed contacts with the bilayer in which MHC-peptide complexes accumulated throughout the contact area—for example, there was no evidence of active clustering (Fig. 5, A and B). FPR was performed with an argon laser beam after the accumulated MHC-peptide complex density in the contacts reached a steady state (*23*). The bleached junctions recovered to initial levels with a $t_{1/2}$ of 5 min (Fig. 5, C and D). Because the only mechanism for fluorescence recovery in the junction was for the accumulated MHC-peptide complexes to disengage from the TCR, the recovery time course provided a measure of molecular turnover in the junction.

In contrast, a markedly different result was observed on MHC-peptide complexes accumulated in the organized immunological synapse formed by 2B4 T cells. Recovery was followed out to 400 s where recovery of >60% was anticipated on the basis of experiments with 2B4 TCR CHO cells. However, no clusters demonstrated any significant recovery in the T cell junctions. Greater than 80% of clusters displayed no detectable recovery at all (Fig. 5, E and F). The bleaching pulse had no apparent effect on the activity of the T cell or on LFA-1 engagement as determined by parallel imaging of normal membrane ruffling and ICAM-1 accumulation. This suggested that MHC-peptide molecules in the central clus-

Table 1. Relative strength of antigens to interactions in solution and T cell contacts. The relative activities and classifications are based on the ability of these ligands to induce apoptosis, IL-2 production, or proliferation of T cells (*4*). Equilibrium and kinetic constants are given (*4*) by injections of soluble MHC molecules presenting the indicated covalently attached peptides over a TCR-coupled biosensor. The half-life ($t_{1/2}$) for a first-order decay process is (ln 2) ÷ k_{off}. Cluster densities and total number of molecules are determined on images acquired at the same resolution for 3.L2 and 2B4 systems (original image element = 0.018 μm²). The 2B4 T cells have twofold as many TCRs as the 3.L2 T cells. Mean of >50 clusters for each point. Equilibrium and kinetic constants were not detected for the null ligands. ND, not determined; molec., molecule.

Ligand	Relative activity	Classification	K_A (mM^{-1})	k_{on} ($M^{-1}s^{-1}$)	$t_{1/2}$ (s)	Density (molec./μm²)	Total no. of molec.
			Cytochrome system				
MCC88-103	100	Agonist	16.6	900	12.1	352	770
T102S	1	Weak agonist	4.2	1,500	1.92	193	310
T102G	<0.001	Antagonist	0.66	3,400	0.14	53	50
K99A	0	Null	ND	ND	ND	<10	<10
			Hemoglobin system				
Hb64-76	100	Agonist	83	5,557	10.8	132	407
N72T	2	Weak agonist	101	15,374	5.10	106	203
N72I	0.006	Antagonist	67	15–25,000	~2.8	68	120
N72A	0.0007	Weak antagonist	–	–	<2.3	34	92
N72E	0	Null	ND	ND	ND	<10	<10

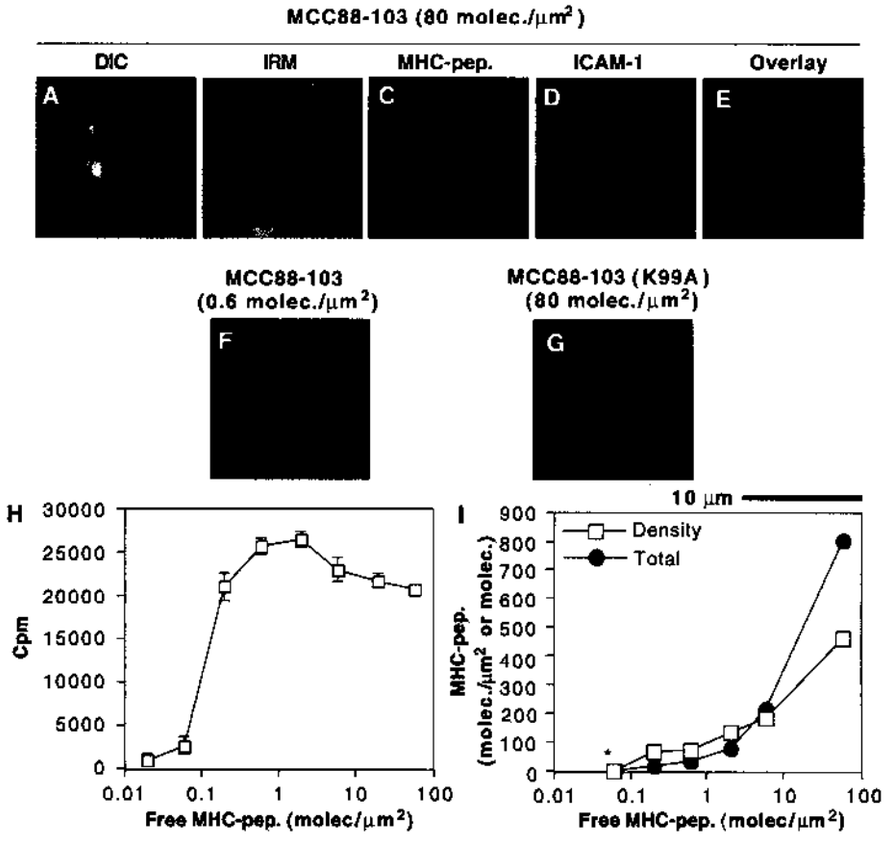

Fig. 2. Immunological synapse formation and MHC-peptide dose. 2B4 T cells on Oregon green E^k-GPI loaded with different peptides and Cy5 ICAM-1–GPI at 200 molecules per square micrometer. Images show accumulated MHC-peptide (green) and ICAM-1 (red). (**A**) to (**E**) E^k(MCC88-103) agonist at 80 molecules per square micrometer. (**A**) Bright-field image; (**B**) IRM image; (**C**) E^k only (green); (**D**) ICAM-1 only (red); (**E**) E^k and ICAM-1 overlay. (**F**) E^k(MCC88-103) agonist at 0.6 molecules per square micrometer E^k plus ICAM-1 overlay. (**G**) E^k(MCC88-103 K99A) null at 80 molecules per square micrometer E^k plus ICAM-1 overlay. (**H**) Dose-response for E^k(MCC88-103) agonist for T cell proliferation on bead-supported bilayers (*41*, *42*). (**I**) Dose-response for E^k-(MCC88-103) agonist for cluster formation at 30 min. The asterisk indicates no immunological synapse formation. Original image elements = 0.018 μm². Data are representative of two experiments.

ter of the immunological synapse were sequestered from the pool of free MHC-peptide complexes and did not exchange, nor were they released from the cluster. These data define a third stage in sustained TCR engagement that we will refer to as "stabilization."

Discussion

To address mechanisms of sustained TCR engagement and fidelity of T cell activation, we examined MHC-peptide accumulation in the immunological synapse using two different TCR systems. We identified three stages for TCR engagement during the formation of a stable immunological synapse: junction formation, MHC-peptide transport, and stabilization (Fig. 6). These stages led to a likely end point for productive TCR engagement: the formation of a stable central cluster. Cluster stabilization was equivalent to formation of a stable immunological synapse. The threshold density of clustered MHC-peptide complexes in forming an immunological synapse was 60 molecules per square micrometer. Having a higher density of MHC-peptide complexes in the central cluster did not correlate with increased T cell proliferation. This indicates that the important event for T cell commitment is the creation of the stable immunological synapse. Thus, synapse formation may be the ultimate (final) stage in which the TCR participates in T cell activation. Monks *et al.* (*11*) were the first to describe the organization of the immunological synapse in fixed cells, but MHC-peptide movement and cluster stability can only be assessed using live cells. Thus, our studies reveal dimensions in the formation of the immunological synapse that were not evident in earlier static images.

The Immunological Synapse Overcomes Barriers to Sustained TCR Engagement

Sustained engagement faces several barriers that are overcome by formation of the immunological synapse. (i) The barrier of the small size of the TCR and MHC-peptide complexes in relation to large glycoproteins is overcome by forcing a ring of T cell membrane against the substrate early in the synapse formation process. Close apposition was maintained as the captured MHC-peptide complexes were transported to the center of the synapse. (ii) The barrier of low affinity is overcome by the tight apposition of this ring of membrane to the substrate that confines the interaction to an attoliter (10^{-18} liter) volume (*24*). (iii) The barrier of rare MHC-peptide complexes is overcome by actively concentrating available complexes by greater than 100-fold in the center of the synapse. This concentration may have been accomplished by active cytoskeletal transport of engaged TCRs that associate with the actin cytoskeleton after interaction with MHC-peptide complexes (*25*). The concentration of MHC-peptide complexes in the central cluster may also drive formation of TCR–MHC-peptide oligomers that could account for the cluster stabilization stage (*5*, *26*). (iv) Finally, the barrier of T cell migration is overcome by the cytoskeletal organization that is an integral part of synapse formation. Directed migration is dependent on the formation of temporary attachments to the substrate that are moved rearward by the actin cytoskeleton (*27*). In contrast, the organization of the immune synapse is radially symmetric and inward directed, such that force vectors cancel and the cells re-

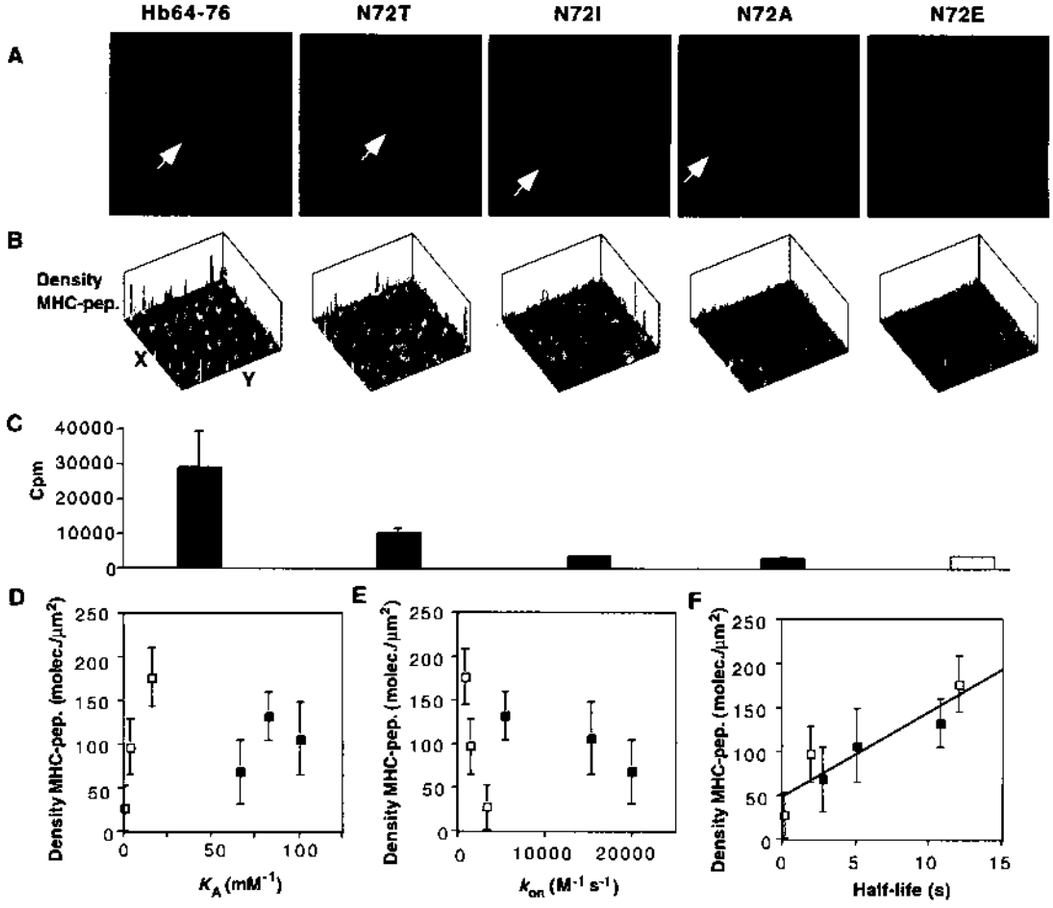

Fig. 3. MHC-peptide cluster density is sensitive to the $t_{1/2}$ of the TCR–MHC-peptide interaction. 3.L2 T cells were incubated with planar bilayers containing E^k and ICAM-1 each at 200 molecules per square micrometer. The E^k was loaded with the indicated peptides at 80 molecules per square micrometer. (**A**) Fluorescence images of MHC-peptide (green) and ICAM-1 (red). (**B**) Perspective view of accumulated MHC-peptide complexes in a representative microscopic field. Red, lowest density; blue, highest density of accumulated MHC-peptide. (**C**) [^{3}H]Thymidine incorporation by 3.L2 T cells in response to planar bilayers with MHC-peptide at 80 molecules per square micrometer and ICAM-1 at 200 molecules per square micrometer. (**D** to **F**) Plots of solution TCR interaction parameters against the density of accumulated MHC-peptide in the cluster for 3.L2 (■) and 2B4 (□). Transgenic T cells express 50,000 2B4 TCRs and 25,000 3.L2 TCRs per cell. Cluster densities were adjusted to 25,000 total TCRs by multiplying the 2B4 cluster density by 0.5. The line in (F) is a linear fit of data from both 2B4 and 3.L2 systems. Original image elements = 0.018 μm^2. Data are representative of two experiments each with 2B4 and 3.L2 systems.

main in place. Thus, the immunological synapse organization is synonymous with the antigen-dependent stop signal (*28*).

MHC-Peptide Clustering Has Fidelity to Early Kinetic Discrimination Processes

Our data also support a role for the immunological synapse in the discrimination of potential antigenic ligands by the TCR. The TCR exhibits an exquisite specificity for its antigen as demonstrated by the significantly different biological outcomes induced by ligands that differ by only a single amino acid. Examination of TCR interaction with MHC-peptide by a panel of altered peptide ligands showed a direct relationship between the process of immunological synapse formation and T cell proliferation. Furthermore, all densities of agonist MHC-peptide complexes that induced T cell proliferation also triggered a central cluster with greater than or equal to 60 molecules per square micrometer of accumulated MHC-peptide complexes. As the number of accumulated MHC-peptide complexes was "locked in" in the final stage of immunological synapse formation, the T cell could thus set a specific threshold to determine whether to commit to the program of T cell activation.

Given the discrete temporal stages of immunological synapse formation, one possible mechanism for T cell discrimination of ligands is based on kinetic models (*29*). Consistent with a kinetic model of T cell activation, we found that the $t_{1/2}$ of the TCR–MHC-peptide interaction correlates with the number of MHC-peptide complexes in the cluster. One process that may contribute to kinetic discrimination is the recruitment of $p56^{lck}$ to the engaged TCR by CD4. The time required to recruit CD4 to the engaged TCR may provide a kinetic window that determines the ability of antigenic peptide complexes to trigger early signals. In contrast, there is no evidence that CD4 participates directly in stabilizing the TCR–MHC-peptide interaction (*30*). The formation of a cluster of MHC-peptide complexes, the size of which is determined by early kinetic discrimination, provides a link between early signaling and later T cell commitment.

These aspects of MHC-peptide strength that determine TCR sensitivity may not only be restricted to kinetics. Although the $t_{1/2}$ of the MHC-peptide complex strongly correlated with central cluster formation and biological response, it is possible that MHC-peptide–induced conformational change in the TCR may also be important (*31*).

A few MHC-peptide complexes can activate a T cell through a process that consumes up to 100 TCRs for each MHC-peptide complex (*32*). This observation is the basis of the "serial engagement" model for T cell activation. Our results are consistent with these data, although we do not directly examine the movement or down-regulation of the TCR. We find that more MHC-peptide complexes are initially captured than are eventually incorporated into the cluster (Fig. 1). On this basis, we speculate that the transport process that moves the MHC-peptide complexes is a barrier to cluster formation and that multiple TCRs may be consumed in the process of transporting a single MHC-peptide complex from the outer ring of the junction to the central cluster. This is consistent with the observation that the transport of MHC-peptide complexes from the outer ring to the central

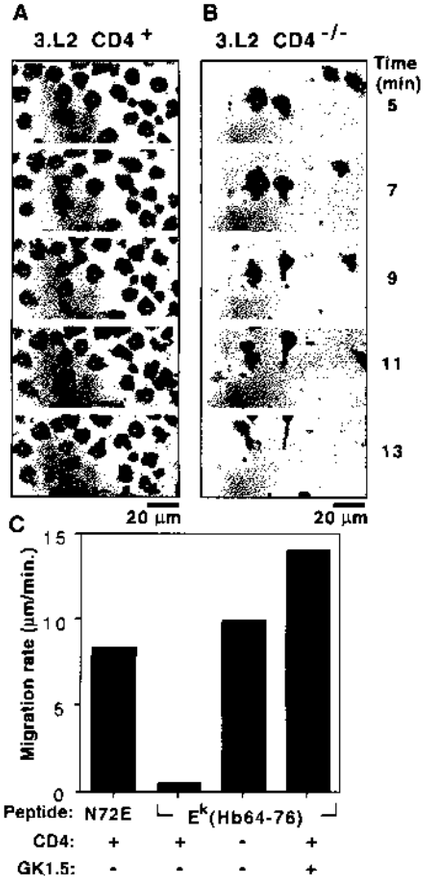

Fig. 4. Role of CD4 in stop signal and MHC-peptide cluster formation. 3.L2 TCR-positive T cells with (**A**) or without CD4 (**B**) were incubated with planar bilayers containing E^k(Hb64-76) at 80 molecules per square micrometer and ICAM-1 at 200 molecules per square micrometer. The time after initial contact is indicated on the right. (**C**) Migration rate of normal 3.L2 and $CD4^{-/-}$ 3.L2 on the indicated substrates. Antibodies were added at 10 μg/ml at 15 min before the injection of cells into the flow cells. Original image elements = 0.44 μm^2. Data are representative of three experiments.

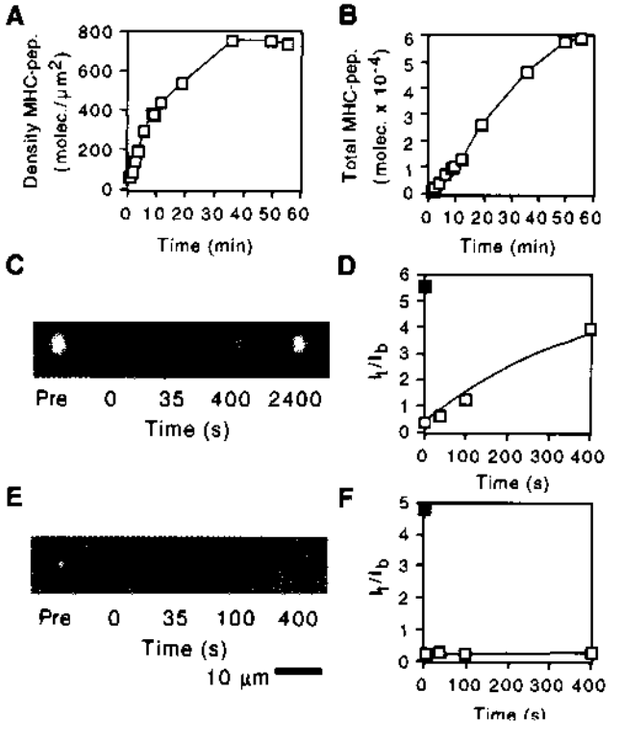

Fig. 5. Dynamics of MHC-peptide clusters generated by TCR-transfected CHO cells and T cells. (A) to (D) 2B4 TCR-GPI–expressing CHO cells on bilayers with E^k(MCC88-103) at 160 molecules per square micrometer. Binding time courses and FPR were done at 22°C. The CHO cells did not form contacts on bilayers with E^k(MCC88-103 K99A) (null peptide). (**A**) Density of accumulated MHC-peptide. (**B**) Total engaged TCR-E^k(MCC88-103) in the contact. Data are from a single contact that is representative of 30 contacts followed in three experiments. (**C**) Contact area fluorescence photobleaching recovery. A steady-state contact was bleached with expanded laser beam at time 0, and the recovery was imaged over 2400 s where recovery was nearly complete. (**D**) Time course of E^k(MCC88-103) turnover in contact area as determined by FPR. Data are representative of six experiments showing >80% recovery. The plotted time course is followed out to the $t_{1/2}$ for recovery of ~400 s. The recovery process is exponential (line). (E) and (F) 2B4 T cell on bilayers with E^k(MCC88-103) at 80 molecules per square micrometer. (**E**) Images of T cell E^k(MCC88-103) cluster bleaching after 30 min at 37°C when the cluster size in junctions reached a steady engaged TCR-E^k(MCC88-103) density. (**F**) Representative recovery time course for a T cell cluster. The average value of recovery is 2% for 20 bleached clusters in three experiments. Original image elements = 0.44 μm^2.

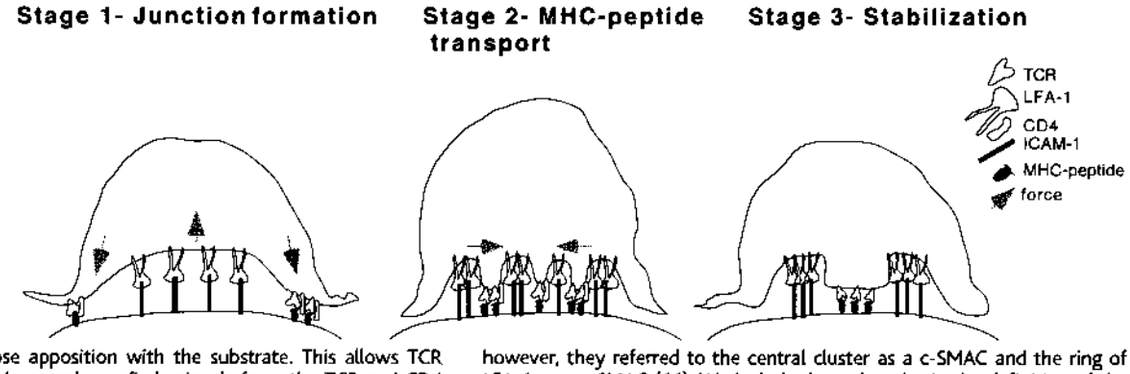

Fig. 6. Model for immunological synapse formation. Side view of T cell forming an immunological synapse with an APC. Stage 1: Junction formation. LFA-1 anchors the central region of the nascent immunological synapse, providing a fulcrum for cytoskeletal protrusive mechanisms that force an outermost ring of T cell membrane into close apposition with the substrate. This allows TCR sampling of MHC-peptide complexes. Early signals from the TCR and CD4 stop migration. Stage 2: MHC-peptide transport. This transport process required ~5 min. We speculate that this is mediated by actin-based transport mechanisms. Stage 3: Stabilization. The clustered MHC-peptide complexes were "locked-in" by an unknown mechanism. The organization of molecules after stage 3 is identical to that reported by Monks *et al.*; however, they referred to the central cluster as a c-SMAC and the ring of LFA-1 as a p-SMAC (*11*). We include these domains in the definition of the immunological synapse, which we observe as a central cluster within two concentric rings. The intermediate ring is enriched in LFA-1–ICAM-1 complexes, whereas the outermost ring of close membrane apposition lacks LFA-1/ICAM-1 complexes, but promotes efficient TCR–MHC-peptide interaction in the nascent synapse.

cluster required minutes, whereas the $t_{1/2}$ of the TCR–MHC-peptide interaction is on the order of seconds. Thus, it is reasonable that it might take several TCRs, engaged in a serial manner, to move the MHC-peptide complexes the required distance of ~5 μm. We nevertheless propose that serial engagement is not an end point where TCRs are spent only in exchange for a transient signal. We show that engaged TCRs are invested in building the stable central cluster. The size of the central cluster relative to a threshold value would then determine longer-term events such as T cell proliferation.

This quantitative analysis reveals how the formation of an immunological synapse provides the machinery to integrate cell surface events into the T cell activation decision. Central cluster formation is based on a transport process sensitive to MHC-peptide strength and number. The intrinsically transient interaction of TCR and MHC-peptide complex is stabilized in the immunological synapse. The MHC-peptide complex must be of sufficient density and potency to attain the stable central cluster, to fully activate the T cell. Thus, building an immunological synapse provides a high-order molecular mechanism to assess MHC-peptide strength with respect to three stages of synapse formation: junction formation (stopping), MHC-peptide transport, and cluster stabilization.

References and Notes

1. E. R. Unanue, *Annu. Rev. Immunol.* **2**, 395 (1984).
2. L. E. Samelson, M. D. Patel, A. M. Weissman, J. B. Harford, R. D. Klausner, *Cell* **46**, 1083 (1986); A. Weiss, R. Shields, M. Newton, B. Manger, J. Imboden, *J. Immunol.* **138**, 2169 (1987); G. R. Crabtree, *Science* **243**, 355 (1989); L. A. Timmerman, N. A. Clipstone, S. N. Ho, J. P. Northrop, G. R. Crabtree, *Nature* **383**, 837 (1996).
3. P. A. van der Merwe, P. N. McNamee, E. A. Davies, A. N. Barclay, S. J. Davis, *Curr. Biol.* **5**, 74 (1995); A. S. Shaw and M. L. Dustin, *Immunity* **6**, 361 (1997).
4. D. S. Lyons *et al.*, *Immunity* **5**, 53 (1996); G. J. Kersh, E. N. Kersh, D. H. Fremont, P. M. Allen, *ibid.* **9**, 817 (1998); S. M. Alam *et al.*, *Nature* **381**, 616 (1996).
5. M. M. Davis *et al.*, *Annu. Rev. Immunol.* **16**, 523 (1998).
6. W. Wang *et al.*, *J. Immunol.* **158**, 5797 (1997).
7. T. A. Springer, *Cell* **76**, 301 (1994).
8. P. M. Allen *et al.*, *Nature* **327**, 713 (1987).
9. E. N. Kersh, A. S. Shaw, P. M. Allen, *Science* **281**, 572 (1998).
10. W. E. Paul and R. A. Seder, *Cell* **76**, 241 (1994); M. L. Dustin *et al.*, *J. Immunol.* **157**, 2014 (1996); M. L. Dustin *et al.*, *Cell* **94**, 667 (1998); C. Wülfing, M. D. Sjaastad, M. M. Davis, *Proc. Natl. Acad. Sci. U.S.A.* **95**, 6302 (1998).
11. C. R. Monks, B. A. Freiberg, H. Kupfer, N. Sciaky, A. Kupfer, *Nature* **395**, 82 (1998).
12. E^k-GPI and ICAM-1–GPI expressed in CHO and BHK cells were solubilized by probe sonication with buffered 1% Triton X-100 and were captured on 14-4-4 or YN1/1 agarose, respectively. Proteins were labeled with Oregon green and Cy5 for E^k-GPI and ICAM-1 (Molecular Probes and Amersham). Labeled E^k-GPI and ICAM-1 were eluted at high pH and were individually reconstituted in phosphatidylcholine (egg) vesicles (*33*). Molecular density was determined by immunoradiometric assays. Iodinated 14-4-4 and YN1/1 were used for E^k-GPI and ICAM-1–GPI, respectively.
13. Web Movies can be seen at www.sciencemag.org/feature/data/1040037.shl.
14. We prepared planar bilayers by mixing the E^k-GPI and ICAM-1–GPI liposomes 1:1 before incubating them on clean glass (*33*) in a parallel-plate flow cell (Bioptechs; Butler, PA). The E^k-GPI was loaded with peptides over 48 hours at 37°C (*34*). Loading of E^k-GPI with MCC88-103 was directly assessed with the D4 monoclonal antibody (mAb) specific to this MHC-peptide complex (*35*). Lower densities of agonist-loaded complexes were generated by mixing in the appropriate null peptide while keeping the total peptide concentration at 100 μM. Cells were injected into the warmed (37°C) flow cells at time zero and then flow was stopped for the duration of the experiment. Thus, any cell movement (migration) is active. The bilayers were imaged as described (*23*).
15. MHC-peptide complexes and ICAM-1 are laterally mobile on APCs (*10*, *36*). Regulation of lateral mobility of MHC-peptide complexes by cytoskeletal interactions augments some T cell responses, but is not essential for T cell activation (*36*).
16. Splenocytes from 2B4 TCR transgenic mice were cultured with 1 μM MCC88-103 peptide for 3 days. The cells were then expanded in media with IL-2 (100 U/ml) and used on day 7. CHO cells expressing GPI-anchored 2B4 TCRs were cultured as described (*37*). Splenocytes from 3.L2 TCR transgenic mice, with or without CD4, were depleted of CD8-positive cells by using magnetic beads (Dynal, Great Neck, NY) and stimulated with 1 μM Hb64-76 peptide. The 3.L2 $CD4^{-/-}$ TCR transgenic cells are selected on the $H\text{-}2^k$ haplotype in the thymus, and normal numbers of mature T cells emerge in the periphery. The peripheral cells were either $CD8^+$, which were depleted here, or double-negative cells, and both populations expressed the clonotypic TCR.
17. C. V. Harding and E. R. Unanue, *Nature* **346**, 574 (1990).
18. The efficiency of E^k loading for different altered peptides was confirmed by competition with the MCC(88-103) peptide as detected by an E^k/MCC-specific mAb, D4 (*35*).
19. A. Kupfer, S. J. Singer, C. A. J. Janeway, S. L. Swain, *Proc. Natl. Acad. Sci. U.S.A.* **84**, 5888 (1987).
20. Proliferation of CD4-negative 3L.2 T cells on planar bilayer was less than one-tenth that obtained with CD4-positive 3L.2 T cells.
21. E. L. Elson, H. Qian, *Methods Cell Biol.* **30**, 307 (1989).
22. In FPR experiments the spot size of an argon ion laser (488 nm) was adjusted to match the fluorescent cluster (*23*, *38*). The cluster was exposed to a brief laser pulse to irreversibly bleach the fluorophores, and the images were acquired with the cooled charge-coupled device camera. The recovery process is a function of both the kinetic rates for the receptor-ligand interaction and the ratio of accumulated fluorescence to the density of free ligand molecules in the bilayer. Thus, these were matched between systems to be compared. The specific cluster fluorescence intensity at a given time (I_t = cluster intensity − bilayer intensity) divided by the fluorescence intensity of ligands in the bilayer (I_b) was plotted against time (*23*, *38*).
23. M. L. Dustin, *J. Biol. Chem.* **272**, 15782 (1997).
24. Data from Fig. 1 were used to estimate the two-dimensional (2D) K_d. FPR showed that 20% of the 50,000 TCRs on 2B4 T cells were laterally mobile. Our analysis considers only mobile TCRs (*39*). We assume that the surface area of the T cell is 500 μm^2. Thus, the 2D K_d = {[80 free E^k(MCC88-103)/μm^2] × [10 free TCRs/μm^2]} ÷ [100 engaged TCR–E^k(MCC88-103)/μm^2] = 10 molecules per square micrometer. The entropy-corrected 3D K_d is 7800 molecules per cubic micrometer (*39*). The 2D K_d ÷ 3D K_d is the confinement region, 1.2 nm in this instance. The volume of the close contact in which TCR engagement occurs is ~5×10^{-17} liters.
25. C. Wülfing and M. M. Davis, *Science* **282**, 2266 (1998); S. Caplan, S. Zeliger, L. Wang, M. Baniyash, *Proc. Natl. Acad. Sci. U.S.A.* **92**, 4768 (1995).
26. Z. Reich *et al.*, *Nature* **387**, 617 (1997).
27. D. P. Felsenfeld, D. Choquet, M. P. Sheetz, *ibid.* **383**, 438 (1996).
28. M. L. Dustin, S. K. Bromley, Z. Kan, D. A. Peterson, E. R. Unanue, *Proc. Natl. Acad. Sci. U.S.A.* **94**, 3909 (1997); P. A. Negulescu, T. B. Krasieva, A. Khan, H. H. Kerschbaum, M. Cahalan, *Immunity* **4**, 421 (1996).
29. T. W. McKeithan, *Proc. Natl. Acad. Sci. U.S.A.* **92**, 5042 (1995); J. D. Rabinowitz, C. Beeson, D. S. Lyons, M. M. Davis, H. M. McConnell, *ibid.* **93**, 1401 (1996).
30. J. J. Boniface *et al.*, *Immunity* **9**, 459 (1998).
31. C. A. Janeway Jr. *et al.*, *Cold Spring Harbor Symp. Quant. Biol.* **54**, 657 (1989); S. M. Alam *et al.*, *Immunity* **10**, 227 (1999).

32. S. Valututti, S. Müller, M. Cella, E. Padovan, A. Lanzavecchia, *Nature* **375**, 148 (1995); A. Viola and A. Lanzavecchia, *Science* **273**, 104 (1996).
33. H. M. McConnell, T. H. Watts, R. M. Weis, A. A. Brian, *Biochim. Biophys. Acta* **864**, 95 (1986); E. Sackmann, *Science* **271**, 43 (1996).
34. D. A. Wettstein, J. J. Boniface, P. A. Reay, H. Schild, M. M. Davis, *J. Exp. Med.* **174**, 219 (1991).
35. K. K. Baldwin, P. A. Reay, L. Wu, A. Farr, M. M. Davis, *ibid.* **189**, 13 (1999).
36. W. F. Wade, J. H. Freed, M. Edidin, *J. Cell Biol.* **109**, 3325 (1989); W. F. Wade, E. D. Ward, E. F. Rosloniec, B. G. Barisas, J. H. Freed, *Int. Immunol.* **6**, 1457 (1994).
37. A. Y. Lin, *et al.*, *Science* **249**, 677 (1990).
38. D. Axelrod, D. E. Koppel, J. Schlessinger, E. L. Elson, W. W. Webb, *Biophys. J.* **16**, 1055 (1976).
39. M. L. Dustin *et al.*, *J. Biol. Chem.* **272**, 30889 (1997).
40. The density and number of accumulated molecules in different regions of the contact area were calculated as the accumulated density (molecules/μm^2) = {[intensity in masked area (fluorescence units/μm^2)] − [intensity in neighboring area (fluorescence units/μm^2)]} ÷ specific activity (fluorescence units/molecule).
41. Planar bilayers with E^k-GPI and ICAM-1–GPI at 200 molecules/μm^2 each were formed on 100-μm glass beads (Mo-Sci, Rolla, MO). Bilayers on large glass beads behave identically to planar bilayers. The E^k on the coated glass beads (25 mg per well) was loaded with peptides as above. Beads were combined with 10^5 rested T cells in 200 μl of RPMI-1640, 10% fetal bovine serum. [^{3}H]Thymidine (0.2 μCi) was added on day 3, the plates were incubated an additional 24 hours, and then the cells were harvested on filters for scintillation counting.
42. D. Gay, C. Coeshott, W. Golde, J. Kappler, P. Marrack, *J. Immunol.* **136**, 2026 (1986).
43. We thank R. Houdei for technical assistance and N. Desai for advice on imaging and data analysis; D. Donermeyer for generation of the 3.L2 TCR transgenic mouse lacking CD4; E. Unanue for inspiring our efforts; E. Elson for help with FPR and the loan of the argon ion laser; J. Heuser and H. Hiyakawa for single-particle imaging; A. Chan, G. Kersh, M. Thomas, E. Unanue, and H. Virgin for critical reading of the manuscript; and J. Smith for final preparation of the manuscript. Supported by grants from the Whitaker Foundation (M.L.D.), the Arthritis Foundation (M.L.D.), the Howard Hughes Medical Institute (M.M.D.), and the NIH (M.L.D., M.M.D., P.M.A, and A.S.S.).

15 March 1999; accepted 1 June 1999

REPORTS

Variations in Atmospheric N_2O Concentration During Abrupt Climatic Changes

J. Flückiger,[1] A. Dällenbach,[1] T. Blunier,[1]* B. Stauffer,[1]† T. F. Stocker,[1] D. Raynaud,[2] J.-M. Barnola[2]

Nitrous oxide (N_2O) is an important greenhouse gas that is presently increasing at a rate of 0.25 percent per year. Records measured along two ice cores from Summit in Central Greenland provide information about variations in atmospheric N_2O concentration in the past. The record covering the past millennium reduces the uncertainty regarding the preindustrial concentration. Records covering the last glacial-interglacial transition and a fast climatic change during the last ice age show that the N_2O concentration changed in parallel with fast temperature variations in the Northern Hemisphere. This provides important information about the response of the environment to global climatic changes.

Nitrous oxide (N_2O) is an atmospheric trace gas with a relatively long lifetime of about 120 years (*1*). The main sources of N_2O in preindustrial times have been tropical soils, the ocean in upwelling regions, and soils in temperate regions (estimated contributions are 45, 30, and 25%, respectively, but with high uncertainties) (*1*). The main sink is photodissociation in the stratosphere (*1*). The atmospheric concentration of this greenhouse gas [which, apart from water vapor, is third in importance after carbon dioxide (CO_2) and methane (CH_4)] reached 314 parts per billion by volume (ppbv) in 1998 (*2*) and increases by about 0.25% per year (*1*). Knowledge about the atmospheric N_2O concentration before 1976 comes mainly from ice core analyses (*3–7*). Our record covering the past millennium allows us to narrow the range of the preindustrial concentration.

Records of CH_4 variations parallel to climatic oscillations have provided a wealth of information about the global significance of climatic oscillations and about the response of the environment to such variations (*8–10*). Like CH_4, N_2O has an important source in the tropics [wet forest soils and dry savannahs for N_2O; wetlands for CH_4 (*1*)], but in contrast to CH_4 it has an important oceanic source too. Therefore, we expect that our measurements, which cover time periods of drastic climate changes, will provide new information about environmental responses to those changes. We present examples from the last glacial-interglacial transition [16.5 to 10.5 thousand years before the present (kyr BP)] and from a fast climate oscillation during the last ice age (37.0 to 32.5 kyr BP).

The air trapped in polar ice samples was extracted with the melt-refreezing method used for CH_4 analyses (*10*, *11*). The N_2O concentration of the extracted air was measured with a gas chromatograph equipped with an electron capture detector. Tests with bubble-free ice and standard gas (the working standard was 304 ± 4 ppbv) confirmed that N_2O can be extracted with the melt-refreezing method despite the high solubility of N_2O in water (*12*), if the freezing speed is kept low. The small sample size (about 40 g) allowed us to measure several samples per annual layer for samples from this millennium as well as one sample per annual layer for the transition from the last glacial epoch to the Holocene. Data presented in this study are not corrected for gravitational fractionation (*13*).

Samples for the first measurement series, covering the past 1000 years (Fig. 1), are from cores drilled at Summit (central Greenland, 72°34′N, 37°38′W) as part of the EUROCORE project and the Greenland Ice Core Project (GRIP). The preindustrial N_2O concentration was relatively stable, with an average of 270 ± 5 ppbv for the time period between 1400 and 1750 A.D. Previously published data (*3–6*) are highly scattered and allow only a rough estimate of the preindustrial concentration of between 260 and 285 ppbv (Fig. 1). An exception are the precise results by Machida *et al.* (*7*) covering the past 300 years. The low scatter of our measurements and the good agreement with the measurements by Machida *et al.*, which were performed with a dry extraction technique, as well as the good agreement with the direct measurements on atmospheric air (*14*) and firn air measurements from Antarctica (*15*), indicate that our measurements for this time period are reliable and allow us to investigate changes in the atmospheric N_2O concentration that occurred together with climatic changes in past climate epochs.

In Fig. 2, the N_2O record for the transition period from the last glacial epoch to the Holocene measured along the GRIP ice core is compared with the GRIP records of oxygen isotope $\delta^{18}O$ (*16*) (used as a proxy for temperature) and CH_4 (*8*, *17*). The N_2O concentration increased

[1]Climate and Environmental Physics, Physics Institute, University of Bern, Sidlerstrasse 5, CH-3012 Bern, Switzerland. [2]CNRS Laboratoire de Glaciologie et Géophysique de l'Environnement (LGGE), Boîte Postale 96, 38402 St Martin d'Hères Cedex, Grenoble, France.

*Present address: Princeton University, Princeton, NJ 08544, USA.

†To whom correspondence should be addressed. E-mail: stauffer@climate.unibe.ch